JOURNAL OF FIELD ROBOTICS

Target localization and pursuit with networked robotic vehicles: theory, simulation, and experiments

SCHOLARONE™
Manuscripts

Accepted

Target localization and pursuit with networked robotic vehicles: theory, simulation, and experiments

Nguyen Hung[1], Eduardo Cunha[1], Francisco Branco[1], Antonio Pascoal[1]

***Abstract*— We address the problem of range-based simultaneous target localization and pursuit (SLAP) with networked robotic vehicles from a theoretical and practical standpoint. The work presented builds upon and extends previous theoretical work by the authors in [1] on the subject of range-based SLAP using multiple trackers and a cooperative distributed estimation and control (DEC) strategy. The key novel contributions of the paper are twofold:**

- **We propose event-triggered communication (ETC) mechanisms for the DEC strategy with formal guarantees of stability of the multiple vehicle ensemble, whereby each tracking vehicle communicates with its neighbors both for target estimation and cooperative control purposes only when deemed necessary, thus reducing the cost of communications, and**
- **to bridge the gap between theory and practice, we analyze the experimental results of numerous field trials with three autonomous marine vehicles with a view to assess the efficacy of the DEC/ETC strategy proposed in a real environment.**

Simulation results are also included and analyzed. For the sake of completeness, we provide source codes and links to auxiliary materials that will enable the readers to run simulations and even implement the DEC/ETC strategy using both Matlab and ROS/Gazebo platforms.
Matlab codes: github.com/hungrepo/slap-etc
ROS packages: github.com/dsor-isr/slap
Aerial view of field trials: youtu.be/4LR4WSJHyz8

***Index Terms*— Target localization, target tracking, distributed estimation, distributed control, event-triggered communications, marine robots, networked systems.**

I. INTRODUCTION

SLAP, which stands for Simultaneous Localization and Pursuit, refers to the task of utilizing one or multiple autonomous robots (trackers) to determine the position of a target (localization) while remaining in a specified vicinity of it (pursuit) [1]–[4]. To accomplish this, the robots are equipped with sensors capable of capturing information about the targets, which is used for localization and pursuit. The sensing information can be obtained through various means, for example acoustic devices for range measurements [1], ultra-short base line (USBL) systems [5], radars [6], and cameras [7] for range and/or bearing measurements. SLAP

holds significant importance due to its applicability in a wide range of practical domains, including search and rescue operations, surveillance tasks, marine animal monitoring and tracking, and underwater aided-navigation, among others [8]–[10].

At the guidance, navigation, and control (GNC) level, SLAP poses a challenging problem in the field of robotics and autonomous systems. This is due to the fact that the estimation of the target's state (localization task) is heavily influenced by the trajectories of the tracking robots (pursuit task), which are determined at the motion planning and control levels. This strong coupling between guidance, navigation, and control necessitates careful attention in the design and analysis process [3], [4], [11], [12].

SLAP and other related problems have been the focus of substantial research in areas at the intersection of estimation, control, and networked systems. The extent of the work done defies a simple summary. For this reason, we refer the reader to the bibliography at the end of the paper and the references therein. Representative examples of SLAP with a single tracker include [3] and [4] using range and bearing measurements, respectively. Due to a number of reasons that include the need to avoid executing very demanding trajectories on the part of the vehicles involved, over the last decade a growing number of strategies addressing the SLAP problem through the utilization of multiple tracking robots have appeared in the literature. However, the prevalent trend is the independent consideration of the two key components involved in the solution of SLAP, with a focus on either the localization or the pursuit task. Noteworthy examples of this approaches appear in [9], [13] for cooperative localization and in [14]–[16] for cooperative pursuit.

When the two tasks (localization and pursuit) are required to be executed simultaneously, the challenge encountered in deploying multiple tracking robots lies in orchestrating their cooperation effectively through the use of an underlying communication network. In response to this challenge, a centralized solution to the multiple tracker SLAP problem using range measurements was introduced in [12]. Subsequently, the same authors introduced recently in [1] a cooperative distributed estimation and control (DEC) strategy to solve the range-based SLAP problem using networked autonomous robots. Inspired by [1], a similar approach was adopted to solve the bearings based SLAP problem in [17].

Contributions: Driven by the fact that the bandwidth available for communication among robots is limited in various practical applications, particularly in underwater environments,

this paper proposes an event-triggered communication (ETC) mechanism for the DEC strategy developed in [1]. The ETC mechanism aims to reduce inter-robot communication while maintaining stability and performance properties comparable to those obtained with continuous communications, albeit with some degradation. This approach draws inspiration from the area of event-triggered communication for distributed control and estimation of multi-agent systems. For a comprehensive explanation of this topic, the readers are encouraged to explore references such as [18], [19] for distributed control and [20], [21] for distributed estimation.

In addition to the theoretical contributions described above, this paper also reports results obtained during numerous field trials with marine robots that show the efficacy and robustness of the proposed algorithms. Codes for ROS packages used for the real trial implementaion is also given, allowing the reader integrate the SLAP algorithm to their robot platform. Finally, for the sake of completeness, we also included simulation results with Matlab, allowing the reader to quickly test and develop applications based on the SLAP algorithm.

The paper is organized as follows. Section II reviews the SLAP problem formulated for networked multiple robots and recalls preliminary results presented in [1]. The proposed ETC mechanisms for the DEC algorithm are described in Section III. Simulation results are included and analyzed in Section IV. Section V reports the results of field trials to assess the efficacy of the DEC/ETC algorithms developed with marine robots developed at IST, Univ. Lisbon. Finally, Section VI contains the main conclusions.

II. PROBLEM STATEMENTS AND PRELIMINARY RESULTS

For readability purposes, this section briefly recalls the SLAP problem and summarizes the key results presented in [1] which will serve as the foundation for the subsequent sections.

A. Problem statement

The SLAP problem considered in [1], illustrated in Fig. II.1 consists of having a group of $N(N \geq 1)$ robots charged with the task of localizing and pursuing a target simultaneously, using only range measurements from the robots to the target. The models of the robots, target, and robots-target sensing information are described next.
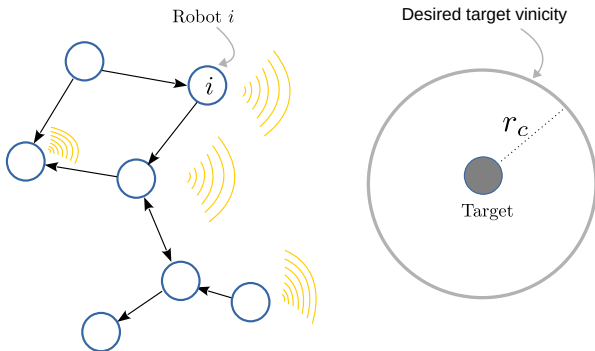
Fig. II.1: Illustration of a SLAP problem. Arrows indicate the flow of information exchanged among the robots.

1) Robots' model: The kinematic model of each robot i is given by

$$\dot{\mathbf{p}}^{[i]} = R(\boldsymbol{\eta}^{[i]})\mathbf{v}^{[i]}, \qquad \dot{\boldsymbol{\eta}}^{[i]} = T(\boldsymbol{\eta}^{[i]})\boldsymbol{\omega}^{[i]}, \qquad (1)$$

where

- $\mathbf{p}^{[i]} \in \mathbb{R}^3$: robot's position in an inertial/world frame $\{\mathcal{I}\}$
- $\mathbf{v}^{[i]}, \boldsymbol{\omega}^{[i]} \in \mathbb{R}^3$: robot's linear and angular velocity vectors, expressed in the robot fixed-body frame $\{\mathcal{B}\}^{[i]}$.
- $\boldsymbol{\eta}^{[i]} \in \mathbb{R}^3$: vector of Euler angles describing the orientation of $\{\mathcal{B}\}^{[i]}$ with respect to $\{\mathcal{I}\}$.
- $R, T \in \mathbb{R}^{3\times3}$: matrices representing linear and angular transformations, see Chapter 2 of [22].

At the kinematic level, $\mathbf{u}^{[i]} \triangleq [\mathbf{v}^{[i]}, \boldsymbol{\omega}^{[i]}]$ is the manipulated input, whose control law is to be found to solve the SLAP problem.

2) Target's model: Let $\mathbf{q}(t) \in \mathbb{R}^3$ be the target's trajectory to be tracked, and $\boldsymbol{v}(t) = \dot{\mathbf{q}}(t)$ the target's velocity, both expressed in $\{\mathcal{I}\}$. Assume that the target undergoes slow changes in velocity, so that $\dot{\boldsymbol{v}} \approx \mathbf{0}$. Under this assumption its discrete- time model adopted for target estimation purposes is given by

$$\mathbf{x}_{k+1} = F\mathbf{x}_k + \mathbf{w}_k, \qquad F = \begin{bmatrix} I_3 & T_s I_3 \\ 0_{3\times3} & I_3 \end{bmatrix}, \qquad (2)$$

where T_s is the sampling period, and $\mathbf{w}_k \sim \mathcal{N}(\mathbf{0}, Q)$.

3) Range measurement model: Assume that each robot i is equipped with an acoustic unit that measures its distance to the target. The range measurement model is given by

$$y_k^{[i]} = d_k^{[i]} + \eta_k^{[i]}, \qquad (3)$$

where $d_k^{[i]}(\mathbf{x}_k) \triangleq \left\| \mathbf{p}_k^{[i]} - \mathbf{q}_k \right\|$ and $\eta_k^{[i]} \sim \mathcal{N}(0, \sigma)$ for all i is Gaussian measurement noise.

4) Robots' network model: In the set up adopted, the robots communicate among themselves using a communication network. In the latter, abstracted as a directional graph (digraph), the set of neighboring robots that robot i can send data to and the set of neighboring robots from which robot i can receive data are denoted $\mathcal{N}_{\text{out}}^{[i]}$ and $\mathcal{N}_{\text{in}}^{[i]}$, respectively. See for example [1] and [23] for fast paced explanations of how this network modeling approach offers many useful algebraic graph properties that are key to the derivation of consensus protocols for cooperative control in the context of the cooperative SLAP problem, stated next.

Cooperative SLAP problem: *Consider the models of the robots, target, range measurement, and inter-robot communication network presented above. Let $\hat{\mathbf{x}}^{[i]}$ denote an estimate of the target's state $\mathbf{x}$ computed by robot i. The SLAP problem is to design a distributed control law for $\mathbf{u}^{[i]}; i \in \mathcal{V} \triangleq \{1, ..., N\}$ and a distributed estimation algorithm for $\hat{\mathbf{x}}^{[i]}; i \in \mathcal{V}$ to fulfill the following tasks:*

- *Cooperative pursuit: ensure that asymptotically all robots stay in a given vicinity of the target, i.e.*

$$\lim_{t\to\infty} \left\| \mathbf{p}^{[i]}(t) - \mathbf{q}(t) \right\| \leq r_{\text{c}}, \qquad (4)$$

- *Cooperative localization (estimation): ensure that all estimates $\hat{\mathbf{x}}^{[i]}$ of the target's sate reach consensus, that*

is,

$$\lim_{k\to\infty} \left\| \hat{\mathbf{x}}_k^{[i]} - \mathbf{x}_k \right\| \leq r_{\mathrm{e}} \tag{5}$$

for all $i \in \mathcal{V}$, where r_c and r_e are desired positive values.

B. Preliminary results

To address the cooperative SLAP problem, the authors in [1] proposed a distributed estimation and control (DEC) architecture shown in Fig. II.2 without the ETC mechanism blocks (the yellow blocks in the figure). These ETC mechanisms represent a novel contribution of the current paper, aiming at reducing communications among the robots, and will be described in the subsequent section.

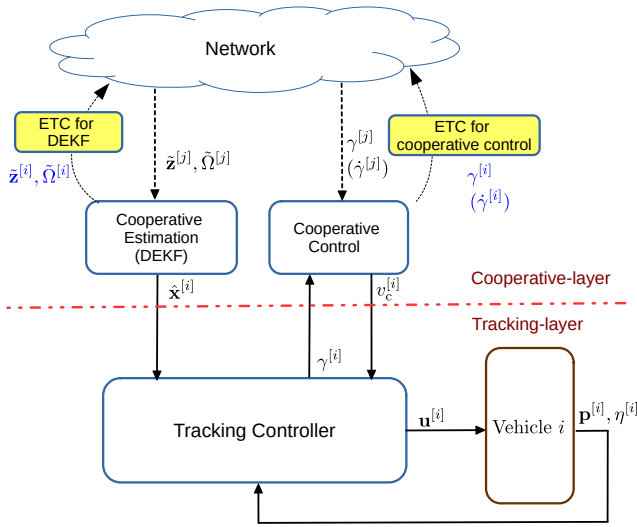In what follows we recall the components of the architecture illustrated in Fig. II.2.

Fig. II.2: The DEC system with ETC mechanisms (yellow blocks) as seen by robot i. In the figure, $j \in \mathcal{N}_{\mathrm{in}}^{[i]}$.

1) Motion planning: At the motion planning level, the main objective is to plan desired trajectories for the robots to track and thereby maintain an optimal geometrical formation relative to the target that, by design, maximizes the range-related information available for target's state estimation purposes. Accordingly, each robot i is a assigned a spatial-temporal (S-T) curve to track in the the form of

$$\mathbf{p}_{\mathrm{d}}^{[i]}(\gamma^{[i]}, t) = \mathbf{r}(\gamma^{[i]}) + \hat{\mathbf{q}}(t), \tag{6}$$

where $\hat{\mathbf{q}}(t)$ is the estimate of the target's trajectory and $\mathbf{r}^{[i]}(\cdot)$ is a corresponding spatial path encircling the target. This path is parameterized by the variable $\gamma^{[i]}$ which is normally chosen as arc-length or normalized arc-length of a circumference. It is important to note that there are no time constraints on the motion of the robot along the spatial path; furthermore, as explained in [1], if the path is parameterized appropriately, then the S-T curves will yield the desired geometrical formations relative to the target when $\gamma^{[i]} = \gamma^{[j]}$ for all $i, j \in \mathcal{V}$. In this context, $\gamma^{[i]}; i \in \mathcal{V}$ are called coordination states and the problem of coordinating the S-T curves to make the coordination states become equal (i.e. to reach consensus) is called a coordination/consensus problem.

2) Cooperative estimation: The main goal of this block is to solve the cooperative localization task given by (5) in a distributed manner. To this end, the authors [1] proposed a distributed EKF (DEKF) whereby each robot i exchanges and fuses a local probability density function (PDF) about the target's state with their neighbors to improve the target's state estimation. In Fig. II.2 the local target's PDF is represented by $\{\tilde{\mathbf{z}}_k^{[i]}, \tilde{\Omega}_k^{[i]}\}$. We refer the reader to Algorithm 2 of [1] for a detailed description of the DEKF algorithm.

3) Cooperative control: At the cooperative control level, the main objective is to coordinate the robots along their assigned S-T curves so as to reach and maintain a desired geometrical formation relative to the target. As described at the motion planning level, this can be achieved if the coordination states $(\gamma^{[i]}, i \in \mathcal{V})$ are equal. For this purpose, the robots exchange and share their local coordination states with their neighbors and apply a local cooperative control in the form

$$v_{\mathrm{c}}^{[i]} = -k_c \sum_{j \in \mathcal{N}_{\mathrm{in}}^{[i]}} (\gamma^{[i]} - \gamma^{[j]}), \tag{7}$$

where $k_c > 0$ is a coupling gain. Here, $v_{\mathrm{c}}^{[i]}$ plays the role of correction speed on the progression of the $\gamma^{[i]}$ to adjust the evolution of the coordination states so that they reach consensus, thereby attaining a desired formation.

4) Tracking control: To track the S-T curves planned at the motion planning level, the authors in [1] proposed two types of tracking controllers, given by equations (49) and (50) of this reference. As shown in [1], these controllers ensure that the robots can track the S-T curve with any arbitrarily tracking error, thereby ensuring that they maintain a desired formation relative to the target.

III. SLAP WITH ETC MECHANISMS

Recall that in order to implement the DEC strategy proposed in [1], each robot is required to exchange continuously the following types of information with their neighbors.

i) The first is associated with the DEKF algorithm that includes messages $\mathcal{M}_{\mathrm{e}}^{[i]}(k)$ given by

$$\mathcal{M}_{\mathrm{e}}(k) \triangleq \{\tilde{\mathbf{z}}_k^{[i]}, \tilde{\Omega}_k^{[i]}\}, \tag{8}$$

where $\tilde{\mathbf{z}}_k^{[i]}, \tilde{\Omega}^{[i]}$ represent the information vector and information matrix associated with a local estimate of the target's distribution, respectively.

ii) The second is associated with the cooperative control law that requires the exchange of messages $\mathcal{M}_{\mathrm{c}}^{[i]}(t) \triangleq \{\gamma^{[i]}(t)\}$. Notice that in general $\mathcal{M}_{\mathrm{c}}^{[i]}(t)$ may also include $\dot{\gamma}^{[i]}(t)$ as shown in Fig. II.2, thus allowing for the use of both proportional and derivative terms in consensus protocols.

In practice, however, continuous communications are virtually impossible via wireless communication networks. A standard way is to transmit $\mathcal{M}_{\mathrm{c}}^{[i]}$ periodically and set the communication period as small as possible in order to achieve a performance comparable to that obtained using continuous communications. To make it simpler for a practical implementation, both messages $\mathcal{M}_{\mathrm{e}}^{[i]}$ and $\mathcal{M}_{\mathrm{c}}^{[i]}$ can be included in one package

and transmitted at the same time, at every sampling interval T_s. In this section, we propose a far more viable approach than continuous or periodic communications that exploits the techniques of event-triggered communications exposed in [24]. Using this setup, it will be shown in the simulation and experimental results sections that the robots only exchange information when necessary, without substantial degradation of the performance achieved with the DEC developed in [1].

A. An ETC mechanism for DEKF

We start by designing an ETC mechanism to decide when a generic robot i must transmit its most recent estimate of the target PDF (stored in message $\mathcal{M}_{\mathrm{e}}^{[i]}$, see (8)) to its out-neighbors $\mathcal{N}_{\mathrm{out}}^{[i]}$. Recall that in order to implement the DEKF each robot i must access periodically the latest local PDFs of the target computed by its in-neighbors $\mathcal{N}_{\mathrm{in}}^{[i]}$. See Fusion step in Algorithm 2 of [1]). The underlying idea behind the ETC mechanism is that if robot i can predict/estimate these PDFs well, then there is no need for its in-neighbors to transmit the densities periodically. To this end, for each robot i we define

$$\bar{p}^{[j]}(\mathbf{x}_k|\bar{\mathbf{x}}_{k-1}^{[j]}, \bar{P}_{k-1}^{[j]}) \sim \mathcal{N}(\bar{\mathbf{x}}_k^{[j]}, \bar{P}_k^{[j]}), \qquad (9)$$

as the estimate of $p^{[j]}$ - the local PDF of the target computed by robot $j, j \in \mathcal{N}_{\mathrm{in}}^{[i]}$. In the expression above $\bar{\mathbf{x}}_k^{[j]}, \bar{P}_k^{[j]}$ denote the estimate of the target state and its associated covariance matrix, respectively. The density $\bar{p}^{[j]}$ can be computed by propagating from the latest density about the target received from robot j through the target model. Formally, let $\{k_l^{[j]}\}_{l\in\mathbb{N}}$ (to be determined by the ETC mechanism) denote the sequence of discrete time instants at which robot j broadcasts $p^{[j]}$ (stored in message $\mathcal{M}_{\mathrm{e}}^{[j]}$). The density $\bar{p}^{[j]}$ is computed as follows. At $k = k_l^{[j]}$:

$$\bar{\mathbf{x}}_k^{[j]} = \tilde{\Omega}_k^{[j]}\tilde{\mathbf{z}}_k^{[j]}, \qquad \bar{P}_k^{[j]} = [\tilde{\Omega}_k^{[j]}]^{-1}, \qquad (10)$$

where the pair $(\tilde{\mathbf{z}}_k^{[i]}, \tilde{\Omega}_k^{[i]})$ parameterizes $p^{[j]}$ - the latest density of the target computed by the robot j (see how to compute this pair in (41) of [1]). During the intervals $[k_l^{[j]}, k_{l+1}^{[j]}), l \in \mathbb{N}$, the density $\bar{p}^{[j]}$ propagates in an open loop manner through the target's model (2), as follows:

$$\bar{\mathbf{x}}_{k+1}^{[j]} = F\bar{\mathbf{x}}_k^{[j]}, \qquad \bar{P}_{k+1}^{[j]} = F\bar{P}_k^{[j]}F^{\mathrm{T}} + Q. \qquad (11)$$

For the sake of clarify, Fig. III.1 illustrates the evolution of the *estimated density* $\bar{p}^{[j]}$ and the *correct density* $p^{[j]}$.

In order to monitor "how well" robot i predicts/estimates the density computed by its neighboring robot j, robot j runs a density *identical* to $\bar{p}^{[j]}$ that is built at robot i with (10) and (11). Thus, the discrepancy between the estimated density $\bar{p}^{[j]}$ and the correct density $p^{[j]}$ at robot i can be monitored by robot j as well. To quantify this discrepancy we adopt a measure, call the Kullback-Leibler Divergence (KLD), defined as

$$\mathcal{KLD}_k^{[j]}(p^{[j]}\|\,\bar{p}^{[j]}) = \frac{1}{2}\mathrm{trace}\left([\bar{P}_k^{[j]}]^{-1}\tilde{P}_k^{[j]} - I_n\right) + ...$$
$$\frac{1}{2}\left\|\bar{\mathbf{x}}_k^{[j]} - \tilde{\mathbf{x}}_k^{[j]}\right\|_{[\bar{P}_k^{[j]}]^{-1}} + \frac{1}{2}\log\left(\frac{\det(\bar{P}_k^{[j]})}{\det(\tilde{P}_k^{[j]})}\right), \qquad (12)$$
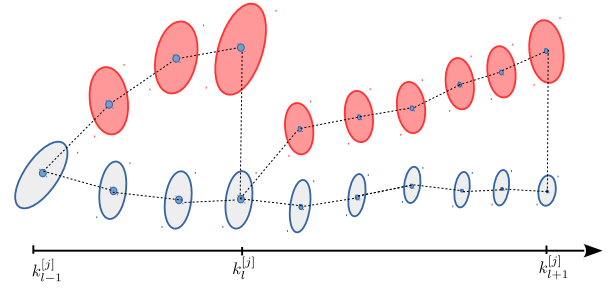

Fig. III.1: Illustration of the *estimated density* $\bar{p}^{[j]}$(red) and the latest *correct density* $p^{[j]}$ (gray). At every $k_l^{[j]}, l \in \mathbb{N}$, $\bar{p}^{[j]} = p^{[j]}$.

where $\tilde{P}_k^{[j]} = [\tilde{\Omega}_k^{[j]}]^{-1}$ and $\tilde{\mathbf{x}}_k^{[j]} = [\tilde{\Omega}_k^{[j]}]^{-1}\tilde{\mathbf{z}}_k^{[j]}$; and n is the dimension of $\bar{\mathbf{x}}_k^{[j]}$ which is identical to the dimension of the target's state [24]. To save communications, the robot j keeps checking $\mathcal{KLD}_k^{[j]}$ and only transmits $p^{[j]}$ whenever this divergence measure exceeds a given threshold. Formally, the robot j will transmit message $\mathcal{M}_{\mathrm{e}}^{[j]}$ that stores $p^{[j]}$ whenever $\mathcal{KLD}_k^{[j]} \geq g^{[j]}(k)$ where $g^{[j]} : k \to \mathbb{R}_{\geq 0}$ is a positive threshold function that is designed to bound the difference between the two densities. Formally, the sequence $\{k_l^{[j]}\}_{l\in\mathbb{N}}$ is specified by

$$k_{l+1}^{[j]} = \inf\{k > k_l^{[j]} : \mathcal{KLD}_k^{[j]} \geq g^{[j]}(k)\} \qquad (13)$$

for all $l \in \mathbb{N}$ and $i = 1, ..., N$.

In summary, with the ETC mechanism presented above, the DEKF with the ETC mechanism for a generic robot i can be implemented with Algorithm 1. In this algorithm, W, V are the inverses of the covariances of process and measurement noises associated with the target and range measurement models given in (2) and (3), respectively, while $\pi^{[i,j]}, \forall i, j \in \mathcal{V}$ are tuning weights in the fusion step. Notice that the latter must be chosen such that $\pi^{[i,j]} > 0$ and $\sum_{j\in\mathcal{N}_{\mathrm{in}}^{[i]}\cup\{\mathrm{i}\}} \pi^{[i,j]} = 1$ for all $i \in \mathcal{V}$.

B. An ETC mechanism for cooperative control

In this section, we propose an ETC mechanism to decide when a generic robot i should transmit message $\mathcal{M}_{\mathrm{c}}^{[i]}$ to its neighbors for coordination control purposes. The ETC mechanism described in this section is inspired by that in [19] and is presented next. Recall that to compute the correction speed $v_{\mathrm{c}}^{[i]}$ given in (7), each robot i needs to assess the variables $\gamma^{[j]}; j \in \mathcal{N}_{\mathrm{in}}^{[i]}$ continuously. In order to overcome this unpractical requirement, robot i will estimate these variables and use their estimates in (7) rather than the true ones. Let $\hat{\gamma}_i^{[j]}$ be the estimate of $\gamma^{[j]}$, estimated by robot i. In the ETC mechanism, the cooperative control law for $v_{\mathrm{c}}^{[i]}$ is given by

$$v_{\mathrm{c}}^{[i]} = -k_c \sum_{j\in\mathcal{N}_{\mathrm{in}}^{[i]}} (\gamma^{[i]} - \hat{\gamma}_i^{[j]}), \qquad (17)$$

where $k_c > 0$. To analyze the ETC mechanism, (17) can be rewritten as

$$v_{\mathrm{c}}^{[i]} = -k_c \sum_{j\in\mathcal{N}_{\mathrm{in}}^{[i]}} (\gamma^{[i]} - \gamma^{[j]} + \tilde{\gamma}^{[j]}), \qquad (18)$$

Algorithm 1 DEKF-ETC for robot i

1: **procedure** INITIALIZATION
2:      At $k = 0$, initialize $\hat{\mathbf{x}}_{1|0}^{[i]}, P_{1|0}^{[i]}$
3:      $\Omega_{1|0}^{[i]} = [P_{1|0}^{[i]}]^{-1}, \quad \mathbf{z}_{1|0}^{[i]} = [P_{1|0}^{[i]}]^{-1}\hat{\mathbf{x}}_{1|0}^{[i]}$
4: **return** $\hat{\mathbf{x}}_{1|0}^{[i]}, \Omega_{1|0}^{[i]}, \mathbf{z}_{1|0}^{[i]}$

5: At each discrete time k, repeat the following procedures:
6: **procedure** CORRECTION
7:      **if** obtain a new range **then**
8:          $C_k^{[i]} = \frac{\partial d_k^{[i]}}{\partial \mathbf{x}}(\hat{\mathbf{x}}_{k|k-1}^{[i]})$
9:          $\tilde{y}_k^{[i]} = y_k^{[i]} - d_k^{[i]}(\hat{\mathbf{x}}_{k|k-1}^{[i]}) + C_k^{[i]}\hat{\mathbf{x}}_{k|k-1}^{[i]}$

$$\tilde{\mathbf{z}}_k^{[i]} = \mathbf{z}_{k|k-1}^{[i]} + (C_k^{[i]})^\top V^{[i]}\tilde{y}_k^{[i]}$$
$$\tilde{\Omega}_k^{[i]} = \Omega_{k|k-1}^{[i]} + (C_k^{[i]})^\top V^{[i]} C_k^{[i]} \qquad (14)$$

10:      **else** set $\tilde{\mathbf{z}}_k^{[i]} = \mathbf{z}_{k|k-1}^{[i]}, \tilde{\Omega}_k^{[i]} = \Omega_{k|k-1}^{[i]}$.

11: **procedure** COMMUNICATION
12:      **if** $\mathcal{KLD}_k^{[i]}(p^{[i]} || \bar{p}^{[i]}) \geq g^{[i]}(k)$ **then**
13:          Broadcast message $\mathcal{M}_{\mathrm{e}}^{[i]}(k)$ given by (8).
14:          Update $\bar{\mathbf{x}}_k^{[i]}, \bar{P}_k^{[i]}$ using (10)
     End

15: **procedure** FUSION (CONSENSUS)

$$\mathbf{z}_{k|k}^{[i]} = \pi^{[i,i]}\tilde{\mathbf{z}}_k^{[i]} + \sum_{j \in \mathcal{N}_{\mathrm{in}}^{[i]}} \pi^{[i,j]}\bar{\mathbf{z}}_k^{[j]}$$
$$\Omega_{k|k}^{[i]} = \pi^{[i,i]}\tilde{\Omega}_k^{[i]} + \sum_{j \in \mathcal{N}_{\mathrm{in}}^{[i]}} \pi^{[i,j]}\bar{\Omega}_k^{[j]} \qquad (15)$$

     return $\mathbf{z}_{k|k}^{[i]}, \Omega_{k|k}^{[i]}, \hat{\mathbf{x}}_{k|k}^{[i]} = [\Omega_{k|k}^{[i]}]^{-1}\mathbf{z}_{k|k}^{[i]}$

16: **procedure** PREDICTION

$$\hat{\mathbf{x}}_{k+1|k}^{[i]} = F\hat{\mathbf{x}}_{k|k}^{[i]}$$
$$\Omega_{k+1|k}^{[i]} = W - WF(\Omega_{k|k}^{[i]} + F^\top WF)^{-1}F^\top W \qquad (16)$$

     return $\hat{\mathbf{x}}_{k+1|k}^{[i]}, \Omega_{k+1|k}^{[i]}, \mathbf{z}_{k+1|k}^{[i]} = \Omega_{k+1|k}^{[i]}\hat{\mathbf{x}}_{k+1|k}^{[i]}$

17: **procedure** PROPAGATE DENSITY $\bar{p}^{[i]}$
18:      Compute $\{\bar{\mathbf{x}}_{k+1}^{[i]}, \bar{P}_{k+1}^{[i]}\}$ using (11)
19: **return** $\bar{\mathbf{x}}_{k+1}^{[i]}, \bar{P}_{k+1}^{[i]}$

---

where

$$\tilde{\gamma}^{[j]} \triangleq \gamma^{[j]} - \hat{\gamma}_i^{[j]}; \quad j \in \mathcal{N}_{\mathrm{in}}^{[i]} \qquad (19)$$

is the estimation error of $\gamma^{[j]}$ computed at robot i. It can be seen that compared with the control law for continuous communications in (7), $v_{\mathrm{c}}^{[i]}$ in (17) has contributions from the above error. The underlying idea in the proposed ETC mechanism is that if this error can be enforced to be bounded then, as we will show later, the coordination error between the robots (i.e. the disagreement among the coordination states) will also be bounded. To make $\tilde{\gamma}^{[j]}; j \in \mathcal{N}_{\mathrm{in}}^{[i]}, i \in \mathcal{V}$ bounded, we define at each robot j the variable $\hat{\gamma}^{[j]}; j \in \mathcal{V}$ as a "replica" of $\hat{\gamma}_i^{[j]}; i \in \mathcal{N}_{\mathrm{out}}^{[i]}$ and keep them synchronized. To this end, their models are proposed as follows.

Let $\{t_n^{[i]}\}; n \in \mathbb{N}$ be the sequence of time instants at which

robot i sends its current value of $\gamma^{[i]}(t_n^{[i]}); n \in \mathbb{N}$ to its out-neighbors. Note that this sequence will be specified by the ETC mechanism. For $\mathcal{T}_n^{[i]} \triangleq [t_n^{[i]}, t_{n+1}^{[i]})$,

$$\dot{\hat{\gamma}}^{[i]}(t) = \bar{\omega}, \qquad (20a)$$
$$\hat{\gamma}^{[i]}(t_n^{[i]}) = \gamma^{[i]}(t_n^{[i]}). \qquad (20b)$$

for all $i \in \mathcal{N}$. Similarly, let $\{t_n^{[ji]}\}; n \in \mathbb{N}$ be the sequence of time instants at which robot $j; j \in \mathcal{N}_{\mathrm{out}}^{[i]}$ receives $\gamma^{[i]}(t_n^{[i]})$. For $\mathcal{T}_n^{[ji]} \triangleq [t_n^{[ji]}, t_{n+1}^{[ji]})$,

$$\dot{\hat{\gamma}}_j^{[i]}(t) = \bar{\omega}, \qquad (21a)$$
$$\hat{\gamma}_j^{[i]}(t_n^{[ji]}) = \gamma^{[i]}(t_n^{[i]}); i \in \mathcal{V}. \qquad (21b)$$

With the above mechanisms, and provided there are no communication delays, i.e. $t_n^{[i]} = t_n^{[ji]}$ for all n and i, then from (20) and (21) we conclude that $\hat{\gamma}^{[i]}(t) = \hat{\gamma}_j^{[i]}(t)$ for all t, i.e. $\hat{\gamma}^{[i]}$ is a copy $\hat{\gamma}_j^{[i]}$. Thus, from (19), the estimation error can be expressed as $\tilde{\gamma}^{[i]} = \gamma^{[i]} - \hat{\gamma}^{[i]}$ for all $i \in \mathcal{V}$. To ensure that the estimation error $\gamma^{[i]}; i \in \mathcal{V}$ bounded, we allow robot i to transmit $\gamma^{[i]}$ whenever this error hits a designed bounded threshold that, in general, can be parameterized by a function of time that we call $h^{[i]}(t)$. Formally, The sequence $\{t_n^{[i]}\}$ is specified by

$$t_{n+1}^{[i]} = \inf\{t > t_n^{[i]} : |\tilde{\gamma}^{[i]}(t)| \geq h^{[i]}(t)\}. \qquad (22)$$

With the ETC mechanism, whenever the robot makes a transmission $\hat{\gamma}^{[i]}$ will be immediately reset to $\gamma^{[i]}$ (see (20b)), it is guaranteed that

$$|\tilde{\gamma}^{[i]}(t)| \leq h^{[i]}(t) \qquad (23)$$

for all t and $i \in \mathcal{V}$. Later, we will show that thanks to (23) the coordination error among the robots will always be bounded and the bound depends explicitly on $h^{[i]}; i \in \mathcal{V}$ (the user designed functions to trade off performance of robots' coordination against the cost of communications). In summary, the proposed ETC mechanism for the coordination purposes can be implemented using Algorithm 2.

Algorithm 2 Coordination with ETC mechanism for robot i

1: At every time t, agent i implements:
2: **procedure** COORDINATION AND COMMUNICATION
3:      **if** $|\tilde{\gamma}^{[i]}(t)| \geq h^{[i]}(t)$ **then**
4:          Broadcast $\gamma^{[i]}(t)$;
5:          Reset $\hat{\gamma}^{[i]}$ using (20b);
6:      **if** Receive $\gamma^{[j]}$ from agent $j \in \mathcal{N}_{\mathrm{in}}^{[i]}$ **then**
7:          Reset $\hat{\gamma}_j^{[i]}$ using (21b);
8:      Run the estimators (20) and (21);
9:      Compute $v_{\mathrm{c}}^{[i]}$ using (17);
10: **return** $v_{\mathrm{c}}^{[i]}$

C. Stability analysis of the complete DEC system with the ETC mechanisms

In order to draw conclusions about the stability of the complete DEC system under the ETC mechanisms, we first examine the stability of the coordination error and pursuit error susbystems.

1) Coordination error system:: Firstly, we study the stability of the coordination error system by extending the analysis in [1]. From (46) and (47) in [1] we obtain

$$\dot{\gamma}^{[i]} = \bar{\omega} + e_\gamma^{[i]} + v_c^{[i]} \overset{(18)}{=} \bar{\omega} + e_\gamma^{[i]} - k_c \sum_{j \in \mathcal{N}_{\text{in}}^{[i]}} (\gamma^{[i]} - \gamma^{[j]} + \tilde{\gamma}^{[j]}).$$

Let $\boldsymbol{\gamma} = [\gamma^{[1]}, ..., \gamma^{[N]}]^{\text{T}}$, with derivative given by

$$\dot{\boldsymbol{\gamma}} = \mathbf{1}\omega + \mathbf{e}_\gamma - k_c L \boldsymbol{\gamma} - k_c \mathcal{A} \tilde{\boldsymbol{\gamma}}, \tag{24}$$

where $\tilde{\boldsymbol{\gamma}} \triangleq [\tilde{\gamma}^{[1]}, ..., \tilde{\gamma}^{[N]}]^{\text{T}}$, and $L, \mathcal{A}$ are the laplacian and adjacency matrices of the digraph respectively, capturing the topology of the inter-vehicle communication network. We now consider the coordination error vector $\boldsymbol{\xi}$ defined by (56) in [1]. Its dynamics in the closed-loop system with ETC mechanism are given by

$$\begin{aligned} \dot{\boldsymbol{\xi}} = W\dot{\boldsymbol{\gamma}} &\overset{(24)}{=} W(\mathbf{1}\bar{\omega} + -k_c L \boldsymbol{\gamma} + \mathbf{e}_\gamma - k_c \mathcal{A}\tilde{\boldsymbol{\gamma}}) \\ &= -k_c L \boldsymbol{\xi} + W\mathbf{e}_\gamma - k_c W \mathcal{A}\tilde{\boldsymbol{\gamma}}. \end{aligned} \tag{25}$$

where W, given by (57) in [1], is used to measure the disagreement between the coordination states. It can be seen that compared with (58) in [1], the dynamic of the coordination error has a new term (the last term), which is contributed by the collective estimation errors of the neighboring coordination states $\tilde{\gamma}$. It is obvious that if the communications are continuous, that is, $\tilde{\gamma} = \mathbf{0}$, then (25) is identical to (58) in [1]. With the ETC mechanism described above, we obtain the following result.

Lemma 1 (stability of coordination system): Consider the coordination error system under the ETC mechanism described by (25). *Assume further that the underlying communication graph is strongly connected. Then, the coordination error system is ISS with respect to the state $\boldsymbol{\xi}$ and the inputs $\mathbf{e}$ and $\mathbf{h} \triangleq [h^{[1]}, ..., h^{[N]}]^{\text{T}}$.*
Proof: See section VII-A.

2) Pursuit error system:: The pursuit error system describes the dynamics of the tracking error of all S-T curves, as defined by (64) in [1]. As stated in Remark 10 [1] the pursuit error system is independent of the correction speed $\mathbf{v}_c$ and hence the ETC mechanism for the cooperative control does not affect on the stability of this system; thus, the Lemma 4 stated in [1] still holds true with the ETC mechanism.
As a consequence, we obtain the following result for the stability of the whole DEC with the ETC mechanisms system.

Theorem 1: Consider the closed-loop complete DEC system composed by the coordination error system and the pursuit error system defined in Lemma 1 and Lemma 4 of [1]. Then, the complete DEC system is ISS with respect to the state $\boldsymbol{\mu} \triangleq [\boldsymbol{\xi}^{\text{T}}, \mathbf{e}^{\text{T}}]^{\text{T}}$ and the inputs $\tilde{\mathbf{x}}$ and $\mathbf{h}$, where $\tilde{\mathbf{x}}$ is the total estimation error of the target state given by (54) in [1].
Theorem 1 follows immediately from Lemma 1 and Lemma 4 of [1] and the stability of cascaded ISS systems [25]. It can be seen that Theorem 2 in [1] is a special case of Theorem 1 when $\mathbf{h} = \mathbf{0}$. In this case the robots communicate continuously to exchange $\mathcal{M}_c^{[i]}$.

IV. SIMULATION RESULTS

This section presents the results of numerical simulations that illustrate the performance of the algorithms proposed for target localization and pursuit. In the simulations, three robots localize and pursue a target in 2D, with the communications among the tracking robots being driven by the ETC mechanisms proposed. The robots' parameters and their inter-communication network are set identical to that in [1]. The threshold functions for the ETC mechanism described in Algorithm 1 is chosen as

$$g^{[i]}(k) = 15e^{-0.05k} + 3, \tag{26}$$

while the threshold function for the ETC mechanism described in Algorithm 2 is set as

$$h^{[i]}(t) = 2e^{-0.05t} + 0.1 \tag{27}$$

for all $i = 1, 2, 3$.

A. 2-D example

The robots´ and the target´s trajectories for the 2-D example are shown in Fig. IV.1. It is clear from Fig. IV.1(a) that the target's positions estimated by the three trackers converge to a small neighborhood of the true target's position. Furthermore, the trackers converge to and stay in a vicinity of the target, while encircling it. This is in agreement with the results plotted in Fig. IV.1(b),that show how all the estimation and pursuit errors converge to neighborhoods of zero.
Fig. IV.2 illustrates the performance of the tracking robots' coordination system. It is visible that the path parameters reach consensus asymptotically and their speeds evolve approximately at the desired speed $\bar{\omega}$, thus yielding tracker coordination along the designated S-T curves.
Fig. IV.3 and Fig. IV.4 contain relevant information regarding the exchange of messages among the tracking robots. Fig. IV.3(a) indicates the time instants at which the robots broadcast messages $\mathcal{M}_c^{[i]} = \{\gamma^{[i]}\}$ associated with the cooperative pursuit task. Fig. IV.3(b) shows clearly that message exchanging among the robots is scarce and occurs only when each of the estimation errors $\tilde{\gamma}^{[i]}$ hits the threshold function $h^{[i]}; i = 1, 2, 3$. In what concerns the communications involved in the cooperative localization task, Fig. IV.4(a) shows the time instants at which the robots broadcast messages $\mathcal{M}_e^{[i]}$, that contain the local pdf of the target estimated by each robot. Fig. IV.4 (b) shows that the robots only transmit the messages to their neighbors whenever the Kullback-Leibler Divergence $(\mathcal{KLD}^{[i]})$ hit the threshold function $g^{[i]}; i = 1, 2.3$.
Compared with the simulation results in [1], it is apparent that the ETC mechanisms reduce the number of communications among the robots while they still guarantee an adequate performance of the target localization and pursuit system.

V. EXPERIMENTAL SETUP AND RESULTS

This section describes the experimental setup developed to field test the DEC/ETC strategy proposed and analyzes the results obtained.
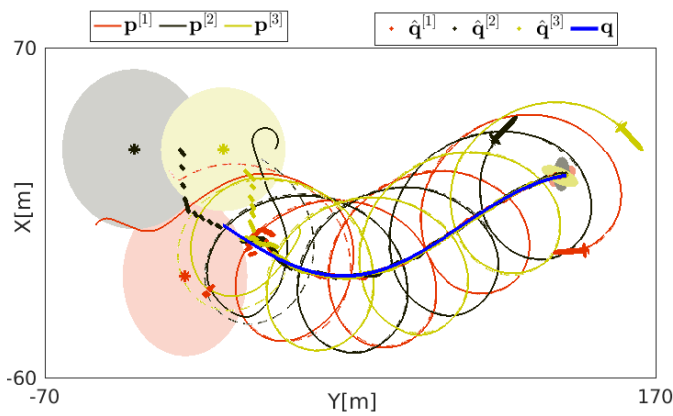
(a) Trajectories: $\mathbf{p}^{[i]}$ (robot), $\mathbf{p}_{\mathrm{d}}^{[i]}$ (S-T curve), $\mathbf{q}$ (target), $\hat{\mathbf{q}}^{[i]}$ (estimated target). The filled initial (large) and final (small) ellipsoids capture, for each tracker, the covariance of target uncertainty estimated by the tracker at the beginning and end of the maneuver, respectively.
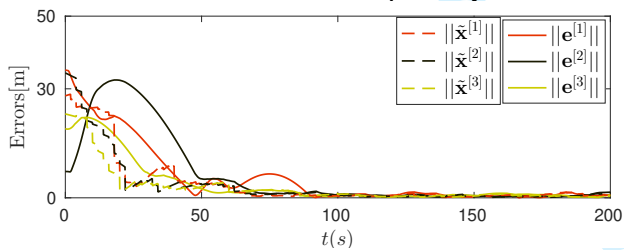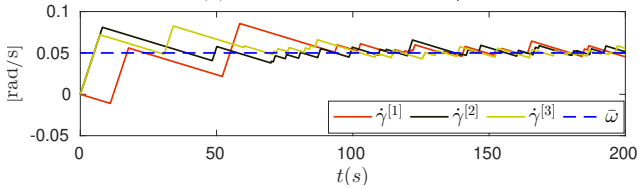

(b) Pursuit errors ($\mathbf{e}^{[i]}$) and localization errors ($\tilde{\mathbf{x}}^{[i]}$).

Fig. IV.1: 2D example - localization and pursuit performance
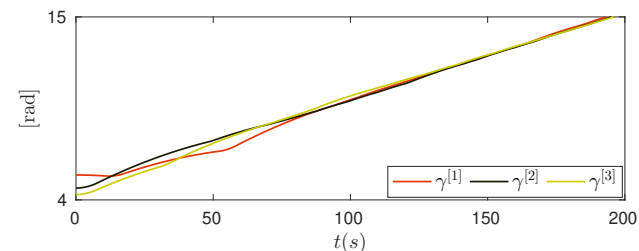
(a) coordination states $\gamma^{[i]}$

(b) Speeds of the coordination state $\dot{\gamma}^{[i]}$.

Fig. IV.2: 2-D example - cooperative pursuit performance

A. Experimental setup

In the experiments performed, two tracking ASVs (autonomous surface vehicles) equipped with ranging devices are responsible for localizing and pursuing a target autonomous underwater vehicle (AUV) undergoing a path following maneuver that is unknown to the trackers, see the diagram in Fig. V.1. The three marine vehicles, built at IST, Univ. Lisbon, are shown in Fig. V.2. Each of the vehicles has the capability to
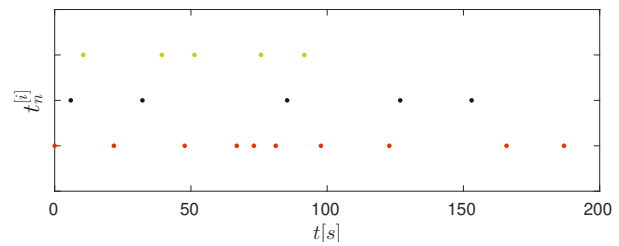
(a) Instants at which the robots broadcast messages $\mathcal{M}_{\mathrm{c}}^{[i]} = \{\gamma^{[i]}\}, i = 1, 2, 3$.
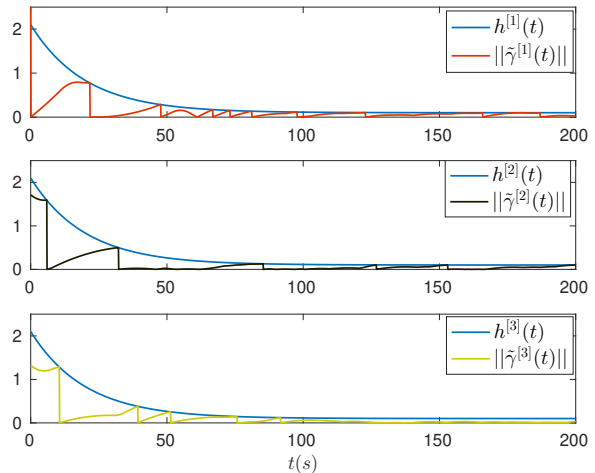

(b) Estimation errors $\tilde{\gamma}^{[i]}$ and the threshold functions $h^{[i]}$.

Fig. IV.3: 2-D example - communications for cooperative pursuit.

run inner control loops and more advanced single and multiple vehicle primitives using the ROS-1 system that supports a proprietary software stack written in C++ and Python. The tracking vehicles communicate via Wifi and measure distances to the target using acoustic ranging devices. For mission programming and mission follow-up purposes, the console shown in Fig. V.3, equipped with a Wifi link to the surface vehicles, is used.

The target vehicle maneuvers at 1.5m depth and navigates using Doppler+AHRS based dead reckoning complemented with position fixes obtained via an inverted USBL complemented with updates on the position of one of the trackers using an acoustic modem. The USBL installed on board the same surface vehicle is used for ground truthing purposes. The DEC/ETC algorithms run on the computers installed onboard the surface vehicles. Notice in Fig. V.4 (obtained with a quadrotor) how the trackers execute the localization and pursuit maneuver by keeping an angle of 90 degrees between the two vectors joining them to the target. This can be achieved by either having the trackers encircle the target or following it from behind (that is, undergoing far less demanding maneuvers), while keeping the same angle, which corresponds to an optimal geometric configuration for target estimation purposes, see [12].
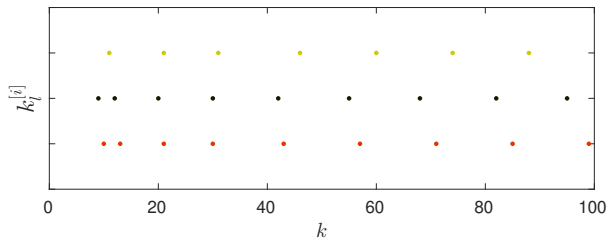
(a) Discrete time instants at which each the robot broadcasts $\mathcal{M}_e^{[i]}$ (the local pdf of the target).
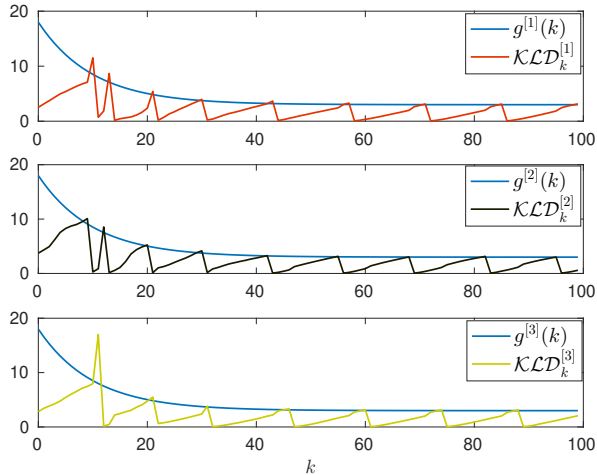
(b) Kullback-Leibler Divergence ($\mathcal{KLD}^{[i]}$), and the threshold functions $g^{[i]}$. Recall that ranges are taken at every k and $t = kT_s$ with $T_s = 2s$ in this simulation.

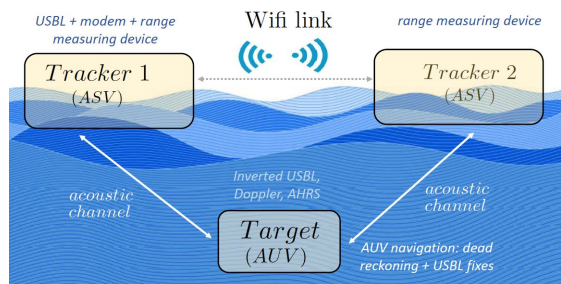Fig. IV.4: 2-D example - communications for DEKF.

Fig. V.1: Setup: two surface robots (trackers), one underwater target, and acoustic range measuring devices.

Fig. V.2: Left to right: target and tracking vehicles.

B. Experimental results

The two trackers' and target's trajectories are depicted in Fig. V.5 with the trackers encircling the target during the

Fig. V.3: Console showing vehicles in operation
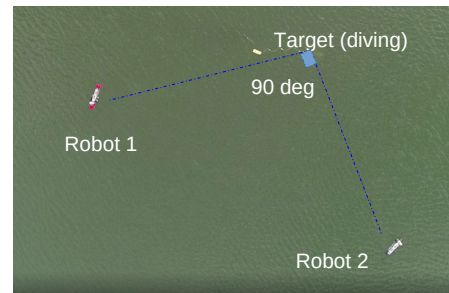
Fig. V.4: Aerial view of the vehicles during a mission.

first part of the maneuver and changing their strategy to follow it during the second part of the maneuver signaled by the "change of formation" caption. The performance of the localization task is illustrated in Fig. V.6 which shows the target state's estimation errors for both trackers converging to within a neighborhood of approximately 1m of the origin. The range measurements from the trackers to the target are shown in Fig. V.7 which confirms that the trackers remain in the set vicinity of the target (8m). The figure also reveals the occurrence of big range measurements which, however, did not impact significantly on the performance of the DEKF because an outlier rejection method was used to process the data acquired before feeding it to the filters.
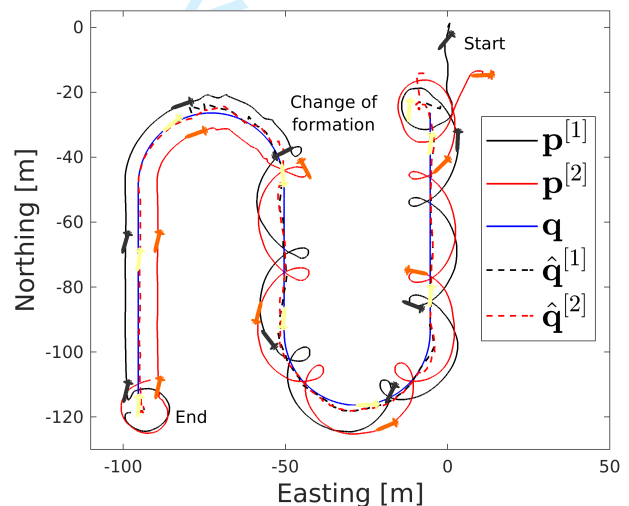

Fig. V.5: $\mathbf{p}^{[i]}$ (trackers), $\mathbf{q}$ (target), $\hat{\mathbf{q}}^{[i]}$ (estimated target).

The two trackers coordination state is also shown in Fig. V.8, implying that they are correctly coordinated along the S-
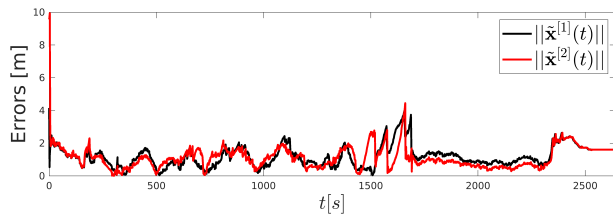
Fig. V.6: Localization errors (difference between the estimated target positions given by the proposed DEC/ETC algorithm and the estimate of the target's position given by the target navigation system.
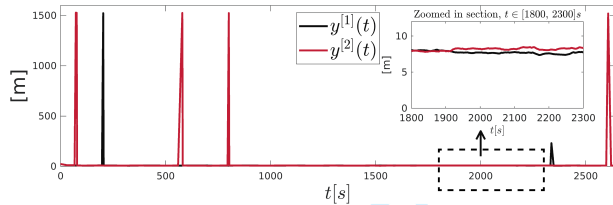

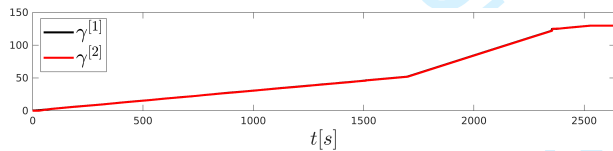Fig. V.7: Range Measurements $y^{[i]}$.

Fig. V.8: Coordination states $\gamma^{[i]}$.

T curves to maintain the desired 90 degree formation. This is confirmed with what is observed in an aerial view captured by a drone, given in Fig. V.4.
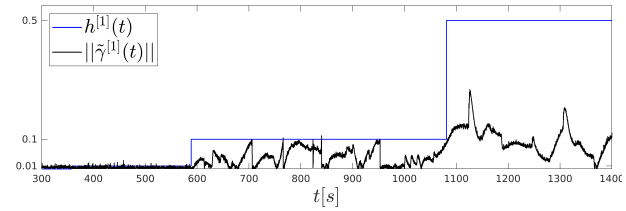
Communications between the trackers for cooperative control and for the DEKF algorithms are shown in Fig. V.9 and Fig. V.10, respectively. For cooperative control, Fig. V.9 shows that each vehicle i only broadcasts the coordination state $\gamma^{[i]}$ when the estimation error hits the threshold function $h^{[i]}$. Similarly, for the DEKF, Fig. V.10 indicates that each vehicle i only broadcasts the local pdf of the target whenever the KLD divergence hits the threshold function $g^{[i]}$. Here, the two threshold functions serve as turning knob used to tradeoff between better cooperative localization and pursuit performance and the cost of communications. It is clear that in both cases, even the larger threshold values guarantee satisfactory performance, while reducing the frequency of communications (Fig. V.9a and Fig. V.10a).

VI. CONCLUSIONS

A methodology was developed to solve the problem of range-based cooperative target localization and pursuit by multiple trackers (autonomous vehicles) using a cooperative distributed estimation and control (DEC) strategy with event-triggered communications (ETC). The latter plays a crucial role in decreasing the average rate of communication between a tracker and its neighbours, as defined by the underlying communications topology. A formal proof of stability of the overall DEC/ETC system was presented. Simulation results were given and discussed and a number of experiments carried
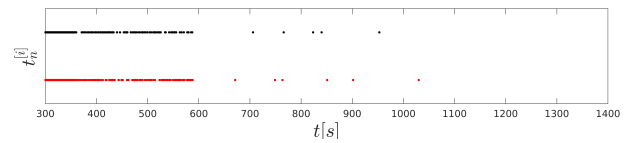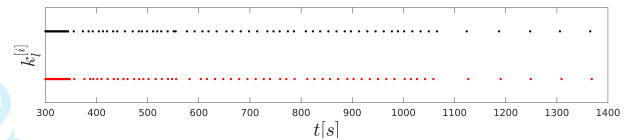

(a) Time instants at which the trackers broadcast $\gamma^{[i]}$.
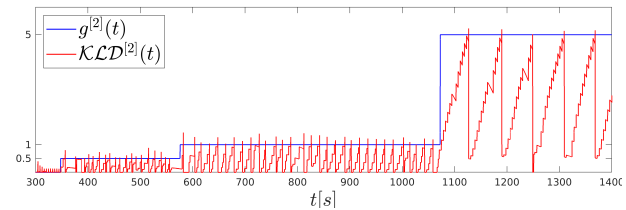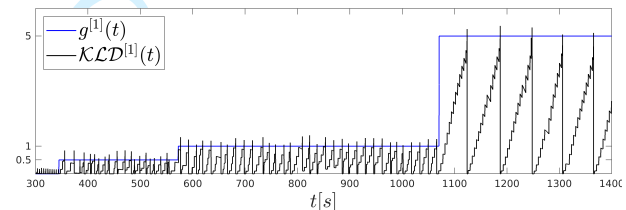

(b) Estimation errors $\tilde{\gamma}^{[i]}$ and threshold functions $h^{[i]}$.

Fig. V.9: Communications for cooperative pursuit.

(a) Time instants at which the trackers broadcast $\mathcal{M}_{\mathrm{e}}^{[i]}$ (the local pdf about the target).

(b) The Kullback-Leibler Divergence ($\mathcal{KLD}^{[i]}$), and the threshold functions $g^{[i]}$.

Fig. V.10: Communications for DEKF.

out with one underwater vehicle (target) performing a path following maneuver and two autonomous surface vehicles (trackers) demonstrated the superior performance of the strategy developed in a real environment.

REFERENCES

[1] Nguyen T. Hung, Francisco F. C. Rego, and António M. Pascoal. Cooperative distributed estimation and control of multiple autonomous vehicles for range-based underwater target localization and pursuit. *IEEE Transactions on Control Systems Technology*, 30(4):1433–1447, 2022.

[2] Brooks Reed, Josh Leighton, Milica Stojanovic, and Franz Hover. *Multi-vehicle Dynamic Pursuit Using Underwater Acoustics*, pages 79–94. Springer International Publishing, Cham, 2016.

[3] Barış Fidan, Soura Dasgupta, and Brian D.O. Anderson. Adaptive range-measurement-based target pursuit. *International Journal of Adaptive Control and Signal Processing*, 27(1-2):66–81, 2013.

[4] Mohammad Deghat, Iman Shames, Brian D. O. Anderson, and Changbin Yu. Localization and circumnavigation of a slowly moving target using bearing measurements. *IEEE Transactions on Automatic Control*, 59(8):2182–2188, 2014.

[5] Benedetto Allotta, Andrea Caiti, Riccardo Costanzi, Francesco Di Corato, Davide Fenucci, Niccolò Monni, Luca Pugi, and Alessandro Ridolfi. Cooperative navigation of auvs via acoustic communication networking: field experience with the typhoon vehicles. *Autonomous Robots*, 40:1229–1244, 2016.

[6] Alfonso Farina. Target tracking with bearings – only measurements. *Signal Processing*, 78(1):61–78, 1999.

[7] J.D. Redding, T.W. McLain, R.W. Beard, and C.N. Taylor. Vision-based target localization from a fixed-wing miniature air vehicle. In *2006 American Control Conference*, pages 6 pp.–, 2006.

[8] Gabriele Ferri*, Andrea Munafò*, Alessandra Tesei, Paolo Braca, Florian Meyer, Konstantinos Pelekanakis, Roberto Petroccia, João Alves, Christopher Strode, and Kevin LePage. Cooperative robotic networks for underwater surveillance: an overview. *IET Radar, Sonar & Navigation*, 11(12):1740–1761, 2017.

[9] Benedetto Allotta, Gianluca Antonelli, Antonino Bongiovanni, Andrea Caiti, Riccardo Costanzi, Daniela De Palma, Paolo Di Lillo, Matteo Franchi, Petrika Gjanci, Giovanni Indiveri, Chiara Petrioli, Alessandro Ridolfi, and Enrico Simetti. Underwater acoustic source localization using a multi-robot system: the damps project. In *2021 International Workshop on Metrology for the Sea; Learning to Measure Sea Health Parameters (MetroSea)*, pages 388–393, 2021.

[10] Manav Kumar and Sharifuddin Mondal. Recent developments on target tracking problems: A review. *Ocean Engineering*, 236:109558, 2021.

[11] N. Crasta, D. Moreno-Salinas, A.M. Pascoal, and J. Aranda. Multiple autonomous surface vehicle motion planning for cooperative range-based underwater target localization. *Annual Reviews in Control*, 46:326 – 342, 2018.

[12] Nguyen T. Hung, N. Crasta, David Moreno-Salinas, António M. Pascoal, and Tor A. Johansen. Range-based target localization and pursuit with autonomous vehicles: An approach using posterior crlb and model predictive control. *Robotics and Autonomous Systems*, 132:103608, 2020.

[13] Bruno M. Ferreira, Aníbal C. Matos, Nuno A. Cruz, and Rui M. Almeida. Towards cooperative localization of an acoustic pinger. In *2012 Oceans*, pages 1–5, 2012.

[14] Mei Yi Cheung, Joshua Leighton, and Franz S. Hover. Decentralized multi-vehicle dynamic pursuit using acoustic tdoa measurements. In *2015 IEEE/RSJ International Conference on Intelligent Robots and Systems (IROS)*, pages 4858–4863, 2015.

[15] Cristino de Souza, Rhys Newbury, Akansel Cosgun, Pedro Castillo, Boris Vidolov, and Dana Kulić. Decentralized multi-agent pursuit using deep reinforcement learning. *IEEE Robotics and Automation Letters*, 6(3):4552–4559, 2021.

[16] Maryam Kouzeghar, Youngbin Song, Malika Meghjani, and Roland Bouffanais. Multi-target pursuit by a decentralized heterogeneous uav swarm using deep multi-agent reinforcement learning, 2023.

[17] Weizhen Wang, Xin Chen, Jiangbo Jia, and Zaifei Fu. Target localization and encirclement control for multi-uavs with limited information. *IET Control Theory & Applications*, 16(14):1396–1404, 2022.

[18] Cameron Nowzari, Eloy Garcia, and Jorge Cortés. Event-triggered communication and control of networked systems for multi-agent consensus. *Automatica*, 105:1 – 27, 2019.

[19] Nguyen T. Hung and Antonio M. Pascoal. Consensus/synchronisation of networked nonlinear multiple agent systems with event-triggered communications. *International Journal of Control*, 95(5):1305–1314, 2022.

[20] Francisco F.C. Rego, António M. Pascoal, A. Pedro Aguiar, and Colin N. Jones. Distributed state estimation for discrete-time linear time invariant systems: A survey. *Annual Reviews in Control*, 48:36–56, 2019.

[21] Giorgio Battistelli and Luigi Chisci. Stability of consensus extended Kalman filter for distributed state estimation. *Automatica*, 68:169 – 178, 2016.

[22] Thor I Fossen. *Handbook of marine craft hydrodynamics and motion control*. John Wiley & Sons, 2011.

[23] Reza Olfati-Saber, J Alex Fax, and Richard M Murray. Consensus and cooperation in networked multi-agent systems. *Proceedings of the IEEE*, 95(1):215–233, 2007.

[24] G. Battistelli, L. Chisci, L. Gao, and D. Selvi. Event-triggered distributed bayes filter. In *2019 18th European Control Conference (ECC)*, pages 2731–2736, 2019.

[25] Eduardo D Sontag. Input to state stability: Basic concepts and results. In *Nonlinear and optimal control theory*, pages 163–220. Springer, 2008.

VII. APPENDIX

A. Proof of Lemma 1

This proof proceeds similarly to the proof of Lemma 3 in [1] as follows. Consider the Lyapunov function candidate $V_c = \boldsymbol{\xi}^\top R \boldsymbol{\xi}/2$, where $R \succ 0$ is a diagonal matrix defined in Lemma 1 of [1]. Taking its time derivative with $\dot{\boldsymbol{\xi}}$ given by (25) yields

$$\dot{V_c} \leq -k_c r_{\min} \|\boldsymbol{\xi}\|^2 + \|\boldsymbol{\xi}\| \left(\|RW\| \|\mathbf{e}_\gamma\| + k_c \|RW\mathcal{A}\| \|\tilde{\boldsymbol{\gamma}}\| \right) \tag{28}$$

Because of (23), $\|\boldsymbol{\gamma}\| \leq \|\mathbf{h}\|$,

$$\dot{V_c} \leq -k_c r_{\min} \|\boldsymbol{\xi}\|^2 + \|\boldsymbol{\xi}\| \left(\|RW\| \|\mathbf{e}_\gamma\| + k_c \|RW\mathcal{A}\| \|\mathbf{h}\| \right).$$

It can be seen that the above equation extends (74) in [1] and therefore, following a procedure similar to that in the proof of Lemma 3 in [1], we conclude that the coordination system is ISS with respect to the state $\boldsymbol{\xi}$ and the inputs $\mathbf{e}$ and $\mathbf{h}$. ∎